



An Analytical Cost Model for Fast Evaluation of Multiple Compute-Engine CNN Accelerators

Fareed Qararyah , Mohammad Ali Maleki , Pedro Trancoso 

Department of Computer Science and Engineering

Chalmers University of Technology and University of Gothenburg, Gothenburg, Sweden

{qararyah, mohammad.ali.maleki, ppedro}@chalmers.se

Abstract—Convolutional Neural Networks (CNNs) serve various applications with diverse performance and resource requirements. Model-aware CNN accelerators best address these diverse requirements. These accelerators usually combine multiple dedicated Compute Engines (CEs). The flexibility of Field-Programmable Gate Arrays (FPGAs) enables the design of such multiple Compute-Engine (multiple-CE) accelerators. However, existing multiple-CE accelerators differ in how they arrange their CEs and distribute the FPGA resources and CNN operators among the CEs. The design space of multiple-CE accelerators comprises numerous such arrangements, which makes a systematic identification of the best ones an open challenge.

This paper proposes a **Multiple-CE accelerator analytical Cost Model (MCCM)** and an evaluation methodology built around MCCM. The model and methodology streamline the expression of any multiple-CE accelerator and provide a fast evaluation of its performance and efficiency. MCCM is in the order of $100000\times$ faster than traditional synthesis-based evaluation and has an average accuracy of $> 90\%$. The paper presents three use cases of MCCM. The first describes an end-to-end evaluation of state-of-the-art multiple-CE accelerators considering various metrics, CNN models, and resource budgets. The second describes fine-grained evaluation that helps identify performance bottlenecks of multiple-CE accelerators. The third demonstrates that MCCM fast evaluation enables exploring the vast design space of multiple-CE accelerators. These use cases show that no unique CE arrangement achieves the best results given different metrics, CNN models, and resource budgets. They also show that fast evaluation enables design space exploration, resulting in accelerator designs that outperform state-of-the-art ones. MCCM is available at <https://github.com/fqararyah/MCCM>

shared by multiple applications [40]. FPGAs' reconfigurability enables the design of accelerators tailored to such diverse requirements, which makes FPGA-based CNN accelerators popular [3], [12], [13], [42], [43], [49].

Accelerators that organize FPGA resources into generic reusable Compute Engines (CEs) have limited adaptability to the varying characteristics of CNN layers, leading to dynamic resource underutilization [5], [29], [30], [41], [50]. This limitation is often described as one size does not fit all. Multiple Compute-Engine (*multiple-CE*) accelerators overcome this limitation. They organize FPGA resources into a number of dedicated CEs tailored to the structure of the CNN model and the available resources [1], [5], [25], [30], [32], [33], [38], [41], [50]. However, the existing multiple-CE accelerators differ in how they arrange their CEs and distribute the FPGA resources and CNN layers among the CEs. Identifying CE arrangements that achieve the best performance and efficiency requires a systematic approach to multiple-CE accelerator design.

A systematic accelerator design approach requires analyzing the *bottlenecks* and inefficiencies and *exploring the design space* to identify optimizations that mitigate them. The literature reveals that the inefficiencies of Deep Learning (DL) accelerators, in general, have three root causes, (1) *Processing Element (PE) underutilization* [4], [23], [48], (2) *large on-chip buffers* [4], [27], [46], (3) and the time and energy costly *off-chip access* [23], [48]. Considering multiple-CE accelerators, the second and third causes are still open challenges. However, multiple-CE accelerators have less PE underutilization than generic ones. Multiple-CE accelerators mitigate PE underutilization bottleneck, but in a way that creates *throughput and latency* trade-off [5], [30], [41]. Hence, a systematic multiple-CE accelerator design approach requires analyzing PE underutilization with latency-throughput trade-offs, on-chip buffer requirements, and off-chip access.

The large design space of CE arrangement possibilities and the lack of a fast methodology that models and evaluates their impact on multiple-CE accelerators' performance and efficiency make a systematic design approach impractical. While High-Level Synthesis (HLS) shortens the design time, synthesizing a single accelerator instance can take hours. To

I. INTRODUCTION

The use of Convolutional Neural Networks (CNNs) in various application domains and across a spectrum of environments, ranging from edge to cloud, brings a wide range of performance requirements and optimization goals [11], [39]. While some applications are latency-critical, others target high throughput. Moreover, resource efficiency is crucial when having limited resources [12], [43], and when resources are

© 2025 IEEE. Personal use of this material is permitted. Permission from IEEE must be obtained for all other uses, in any current or future media, including reprinting/republishing this material for advertising or promotional purposes, creating new collective works, for resale or redistribution to servers or lists, or reuse of any copyrighted component of this work in other works.

overcome this challenge, this paper proposes a Multiple-CE accelerator analytical Cost Model (MCCM), and an evaluation methodology built around it. The proposed model and methodology enable the expression of any multiple-CE accelerator using simple notation and provide a fast and accurate evaluation of its throughput, latency, on-chip buffer requirements, and off-chip accesses. This paper makes the following contributions:

- It proposes a multiple-CE accelerator analytical cost model (MCCM). MCCM applies bottom-up modeling of the impact of CE arrangement possibilities on the performance and efficiency of multiple-CE accelerators.
- It proposes MCCM-based evaluation methodology, which enables expressing any multiple-CE accelerator and evaluates its latency, throughput, on-chip buffer requirements, and off-chip accesses orders of magnitude faster than the traditional approach.
- It presents three use cases of MCCM. First, an end-to-end evaluation of state-of-the-art multiple-CE accelerators considering different metrics, CNNs, and resource budgets. Second, fine-grained evaluation of multiple-CE accelerators' performance bottlenecks. Third, a design space exploration of multiple-CE accelerators enabled by MCCM fast evaluation.

MCCM is in the order of $100000\times$ faster than synthesis-based evaluation and has an average accuracy of $> 90\%$. The presented MCCM use cases using three state-of-the-art multiple-CE accelerators, five CNNs, and four FPGA boards show that no single multiple-CE architecture is the best given different metrics, CNN models, and resource budgets. Moreover, the evaluation shows the impact of engine arrangements on multiple-CE accelerators' performance bottlenecks. Finally, using MCCM fast evaluation as a basis for multiple-CE accelerators design space exploration enables identifying designs that outperform the state-of-the-art.

II. BACKGROUND AND MOTIVATION

A. Convolutional Neural Networks (CNNs)

Convolutional Neural Networks (CNNs) are feed-forward Deep learning (DL) algorithms [20]. A CNN comprises a sequence of *layers*, that perform feature extraction and classification [21]. Convolutional layers are the primary layers in a CNN. A convolutional layer consists of a collection of trainable parameters, known as *weights*, which are organized into *filters*. These filters extract features from multi-dimensional inputs or intermediate results. The inputs of a layer are referred to as Input Feature Maps (*IFMs*), and the outputs as Output Feature Maps (*OFMs*). The term Feature Maps (*FM*s), or activations, refers to both IFMs and OFMs. FMs consist of 2D slices known as *channels*.

B. CNN Compute-Engines

As convolutions represent more than 90% of modern CNN operations [23], CNN Compute-Engine (CE) optimizations focus on convolutional layers. A CE comprises a grid of Processing Elements (PEs) where each PE performs a MAC operation, e.g. a DSP in an FPGA. Two main design decisions that

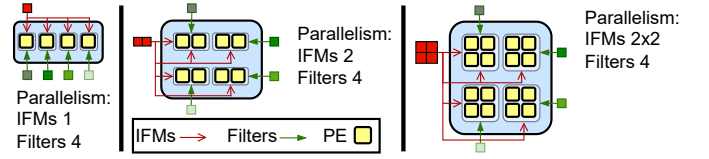


Fig. 1. Compute-Engine (CE) parallelism examples

affect the performance and efficiency of a CE are *parallelism strategy* and *dataflow*. A convolution operation comprises a loop nest of six loops, without batching [17]. A CE parallelism strategy describes which among these six loops are partially or fully parallelized. The CE parallelism strategy affects data reuse and memory access patterns [8], [23]. Figure 1 depicts examples of parallelism strategies in 3-D, 2-D, and 1-D. An exhaustive analysis of parallelism strategies on FPGAs shows that parallelizing on three dimensions, namely across filters and within an IFM channel width and height, yields the best average reuse and CE utilization across the layers of common CNNs [23]. However, 2-D and 1-D parallelism are also common when each CE has a limited PEs budget, or when 1-D or 2-D options are more compatible with the dimensions of the CNN layers processed by that CE [1], [24], [33], [37], [47], [49], [50]. In the context of convolution CEs, the term *dataflow* refers to both convolution loop transformations, *i.e.* the scheduling of the loops computations, and the mapping of computations across the CE PEs. The most common dataflow types are *weight-stationary*, *output-stationary*, and *input-stationary*. Each dataflow indicates which of the IFMs, OFMs, or weights is scheduled to move least frequently [18].

C. Multiple compute-engine CNN accelerators

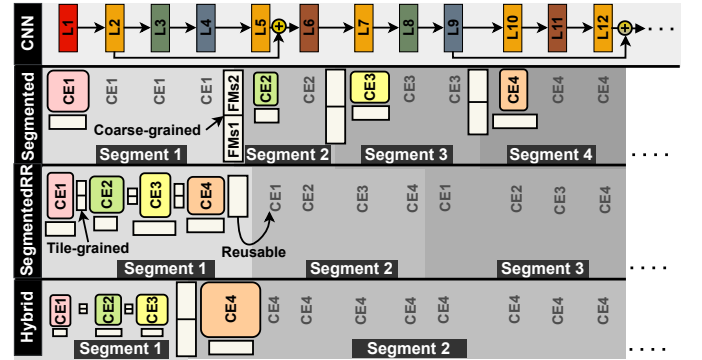


Fig. 2. CNN to multiple-CE architecture mapping examples. For example, in Segmented, CE1 processes layers L1-L4, CE2 processes layers L5 and L6, and so on. In practice, CE and buffer sizes are proportional to the segment layers' compute and memory requirements respectively

We use the term multiple Compute-Engine (*multiple-CE*) accelerators to refer to accelerators that organize the FPGA resources into more than one convolution CE. The extreme case of multiple-CE architecture is to have a CE per CNN layer tailored to that layer's characteristics. This approach is resource-demanding and not scalable [5], [30], [50]. To be both CNN model-aware and scalable, state-of-the-art multiple-CE accelerators adjust the number of CEs based on the CNN

TABLE I
COMPARISON OF MULTIPLE-CE ACCELERATORS USING RESNET50 ON
AMD ZYNQ 7000 SoC ZCU102. THE VALUES FOR A METRIC ARE
NORMALIZED TO THE BEST IN THAT METRIC.

	latency	on-chip buffers	off-chip accesses
SegmentedRR	1.0	2.64	1.79
Segmented	4.7	1.0	1.99
Hybrid (b)	1.11	1.74	1.0

characteristics and the available FPGA resources. Exploring the literature shows that, apart from the mentioned extreme case, multiple-CE accelerators follow one of three architectural patterns. Figure 2 shows a high-level representation of these architectures using four CEs. In practice, the number of CEs varies depending on the CNN structure and the available resources. Each of these CEs may have a unique number of PEs, parallelism strategy, and dataflow (Section II-B).

We refer to the first architecture in Figure 2 as **Segmented** [32], [33]. In this architecture, each CE processes one or more *segments*. Each segment consists of a set of consecutive layers. Each CE has its on-chip buffer that stores the weights and FMs partially or fully depending on the available on-chip memory. *Coarse-grained pipelining*, where different CEs process different inputs (images) at a certain time step, is applied between the CEs. CE inputs are double-buffered to enable pipelining. We call the second architecture **SegmentedRR** (round-robin) as CEs in such architecture usually process CNN layers circularly according to their topological order [3], [38], [41]. While some apply coarse-grained pipelining between CEs, Wei *et al* [41] have shown that, for this architecture, *tile-grained pipelining* is more efficient. In addition to the double-buffering between the CEs, each CE has a separate buffer for the weights. We call the third architecture **Hybrid** [1], [25], [30], [50]. It comprises two parts. The first contains a set of tile-grained pipelined CEs each processing a single layer. The second has a larger CE that processes the rest of the layers. If the CNN has two types of convolutional layers the second part could have two sub-CEs [30]. Coarse-grained pipelining is applied between Hybrid’s first and second parts.

D. Multiple-CE accelerator modeling and evaluation

State-of-the-art multiple-CE accelerators adopt one variant of the three mentioned architectures and focus on optimizing over two extremes, namely reusable-CEs based accelerators [2], [23], [45] and accelerators with as many CEs as CNN layers [36], [49]. Adopting fixed architectures limits the potential of existing multiple-CE accelerators. No single architecture is optimal when considering different metrics. Table I, which reports normalized synthesis results of instances of the three architectures, exemplifies that. For example, the SegmentedRR at the first row has the best latency but requires $2.64\times$ the on-chip buffer and $1.79\times$ the off-chip accesses of the best accelerator in each metric. Note that buffer requirements and off-chip memory accesses are treated here as optimization goals. This is because minimizing off-chip accesses, consequently bandwidth requirements, and on-chip buffer requirements are crucial, especially when resources

are shared by multiple applications [40], even when neither of them forms a bottleneck. The fact that no single architecture gives the best results considering different metrics, even for the same CNN and FPGA as the table shows, suggests that a fixed architecture is far from optimal. Hence, a more systematic design approach that explores different CE arrangement possibilities is needed to identify the best designs given an application performance metrics, CNN model, and resource budget. However, a traditional evaluation of one CE arrangement can take hours. This makes exploring the numerous CE arrangement possibilities of multiple-CE accelerators, and consequently a systematic design approach, impractical. This motivates proposing a fast evaluation methodology of multiple-CE accelerators.

III. MULTIPLE-CE ACCELERATOR EVALUATION METHODOLOGY

A. Overview of the evaluation methodology

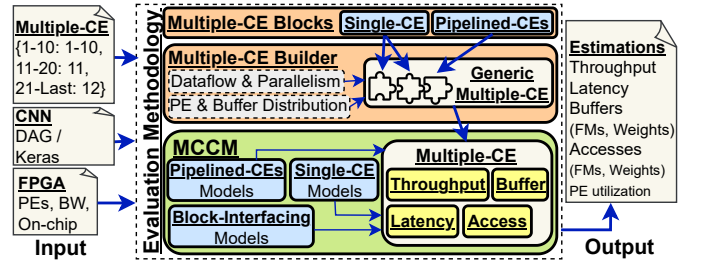


Fig. 3. Overview of multiple-CE evaluation methodology.

Figure 3 presents an overview of the proposed multiple-CE accelerator evaluation methodology. The methodology takes as **inputs**: (1) multiple-CE accelerator description, discussed in the Section III-B, (2) a CNN representation, (3) FPGA’s number of PEs (DSPs), off-chip memory bandwidth, and on-chip memory capacity. The main **outputs** are throughput, latency, on-chip buffer requirements, and off-chip accesses. Other outputs include a fine-grained analysis of PE utilization and a breakdown of the results on the level of weights and FMs. The evaluation methodology comprises three modules. The **Multiple-CE Blocks** module contains codified descriptions of two building blocks that could be used to construct any multiple-CE accelerator, namely *single-CE* and *pipelined-CEs*. A building block comprises one or more CEs. The **Multiple-CE Builder** module constructs a *generic multiple-CE accelerator* backbone by combining the building blocks considering the three methodology inputs. It then decides the implementation details, including the CEs buffer and PE distribution, dataflows, and parallelism strategies based on a set of heuristics inspired by the prior art [3], [23], [30], [33], [41]. The **MCCM** module evaluates a generic multiple-CE accelerator bottom-up by modeling its building blocks and their interfaces. MCCM estimates multiple-CE accelerator throughput, latency, on-chip buffers, and memory access requirements. MCCM is the main contribution of this work; hence, we use the terms MCCM and evaluation methodology interchangeably. As DL

accelerator design is a hot topic where new accelerators are frequently proposed, we designed MCCM to be modular and extensible. MCCM interface allows easy addition of models of newly proposed specialized designs. MCCM components are discussed in detail throughout Section IV.

B. Expressing a generic multiple-CE accelerator

Examining existing multiple-CE accelerators, shown in Figure 2, shows that they comprise two basic building blocks. The first is a *single-CE processing a range of layers* one by one. For example, CE_1 processing layers $L_1 - L_4$ in the Segmented, and CE_4 processing L_4 to the last layer in the Hybrid. The second building block is a set of *pipelined-CEs, each processing a layer*. For example, $CE_1 - CE_4$ processing layers $L_1 - L_4$ in SegmentedRR, and $CE_1 - CE_3$ processing layers $L_1 - L_3$ in Hybrid. These two blocks could be used to express any multiple-CE architectures. We propose the following notation to express a multiple-CE architecture:

- CE_x : denotes a single-CE block, and $CE_x - CE_y$: denotes $(y - x) + 1$ pipelined-CEs block.
- $\{L_x - L_y : CE_z\}$: denotes that layers x to y are processed using a single-CE block (CE_z) sequentially. A special case is having one layer only, namely $\{L_x : CE_z\}$.
- $\{L_x - L_y : CE_z - CE_w\}$: denotes that layers x to y are processed using pipelined-CEs block. If the number of layers exceeds the number of CEs, the pipelined-CEs block is assumed to process $(w - z) + 1$ layers at a time.

For example, the Segmented accelerator in Figure 2 is expressed as $\{L_1 - L_4 : CE_1, L_5 - L_6 : CE_2, L_7 - L_9 : CE_3, L_{10} - L_{12} : CE_4, \dots\}$, and the SegmentedRR can be expressed as $\{L_1 - Last : CE_1 - CE_4\}$. Multiple-CE Builder transforms this notation, given the CNN and FPGA descriptions, into a generic multiple-CE accelerator representation that is fed into the analytical cost model.

IV. MULTIPLE-CE ACCELERATOR ANALYTICAL COST MODEL

The Multiple-CE accelerator analytical Cost Model (MCCM) models a generic multiple-CE accelerator using a bottom-up approach. It evaluates the accelerator using the models of the single-CE and pipelined-CEs blocks and the interfaces between them. The blocks modeling is discussed in Sections IV-A. Modeling a whole accelerator depends on (1) whether each of its blocks processes multiple segments (like the pipelined-CEs block in the SegmentedRR in Figure 2) or one segment (like single-CEs blocks in the Segmented in Figure 2) and (2) whether there is an inter-segment pipelining (like in the Segmented in Figure 2) or not. The details of such dependencies are discussed in Section IV-B.

A. Modeling multiple-CE accelerator building blocks

This section presents the modeling of the single and pipelined-CEs' blocks. Figure 4a and 4b illustrate the differences between processing three convolutional layers using the two blocks. Figure 4a depicts the single-CE case. In this case, each layer is processed to completion before moving to the

next. Figure 4b depicts the pipelined-CEs case. In this case, the layers are processed concurrently, stage by stage, at tile granularity. The figure shows four out of the six stages.

1) *Latency and throughput*: In the *single-CE* case, the latency of processing a set of layers is the sum of their latencies, and the throughput is its inverse. For simplicity, we assume that all layers are compute-bound and that the memory access time is completely hidden by computation time throughout the discussion. In practice, however, we do consider memory access time. Equation 1 describes latency estimation considering PE underutilization, where *layers* is the number of layers processed by the single-CE, *DD* is the disjoint dimensions of the filters and FMs, i.e. the six dimensions corresponding to the six convolution loops (Section II-B), and $Par(CE_j, d)$ is the parallelism on a dimension d . The parallelism across all dimensions is upper-bounded by the number of PEs of a CE. To explain the PE underutilization, consider the single-CE shown in Figure 4c with the parallelism of 16 ($4 \times 2 \times 2$). This CE processes weights from 4 filters and a 2×2 IFM tile in a cycle. When this CE is used to process L2 from Figure 4a, which has 6 filters, its PEs are fully utilized when processing the first 4 filters and half utilized when processing the remaining 2. The parallelism dimensions could be configured differently to avoid underutilization in L2, but such arrangements would result in underutilization in the other layers. Generally, the more diverse the layers processed by a single-CE are, the harder it is to avoid PE underutilization.

$$\begin{aligned}
 Latency &= \sum_{i=1}^{layers} Lat(L_i, CE_j) \\
 Lat(L_i, CE_j) &= \prod_{d \in DD_i} \lceil |d| / Par(CE_j, d) \rceil \\
 &\text{where } \prod_{d \in DD_i} Par(CE_j, d) \leq PEs(CE_j)
 \end{aligned} \tag{1}$$

The literature defines the latency of *pipelined-CEs* in two ways. The first is the time to process a single input, e.g., an image. The second is the time to process a batch of inputs divided by the number of inputs. Here, we adopt the first definition because batching is not always an option and because the first definition is the one that matters in latency-critical applications. Equation 2 shows latency estimation of pipelined-CEs, where *PipeStages* is the number of stages to complete processing an input, *CEs* is the number of CEs in the pipeline, $FMsTile_{ij}$ is the FMs tile processed at stage i by CE_j , and $activeCEs(stage_i)$ are CEs active at stage i . Figure 4b visualizes stages and CE activity. The interpretation of the equation is that the latency of processing a set of layers is the summation of the pipeline stage latencies, and the stage latency depends on the slowest active CE in that stage.

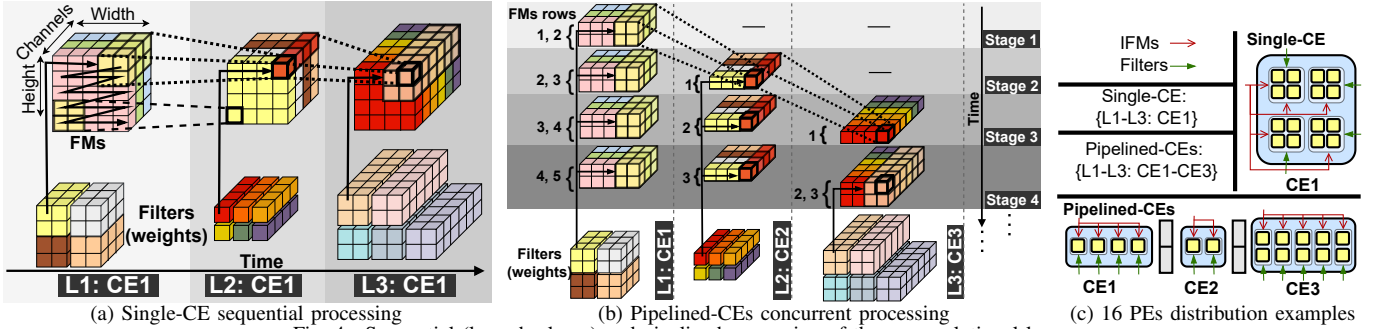


Fig. 4. Sequential (layer by layer) and pipelined processing of three convolutional layers

$$\begin{aligned}
 \text{Latency} &= \sum_{i=1}^{\text{PipeStages}} \text{Lat}(\text{stage}_i) \\
 \text{Lat}(\text{stage}_i) &= \max_{j=1}^{CEs} \left(\text{Lat}(\text{FMsTile}_{ij}, \text{CE}_j) \right) \\
 &\text{where } \text{CE}_j \in \text{activeCEs}(\text{stage}_i)
 \end{aligned} \quad (2)$$

Equation 3 depicts pipelined-CEs throughput estimation where CE_Stages_i denotes the stages in which CE_i is active. Pipeline throughput is the inverse of the slowest CE latency [49]. To maximize the throughput of pipelined-CEs, the slowest CE's latency must be minimized. This is done by balancing the pipeline stages, *i.e.* assigning PEs to each CE proportional to its relative workload [3], [49].

$$\begin{aligned}
 \text{Throughput} &= \frac{1}{\max_{i=1}^{CEs} \left(\text{Lat}(L_i, \text{CE}_i) \right)} \\
 \text{Lat}(L_i, \text{CE}_i) &= \sum_{j=1}^{\text{CE_Stages}_i} \text{Lat}(\text{FMsTile}_{ij}, \text{CE}_i)
 \end{aligned} \quad (3)$$

The pipelined-CEs example in Figure 4c demonstrates how distributing the PEs on multiple CEs could solve the PE underutilization. Each CE in the figure has a parallelism that perfectly divides the corresponding layer filters and FM dimensions. As a result, the pipelined design has an overall higher throughput than the single-CE. However, this comes at the cost of often higher latency. While improving PE utilization results in lower average latency per operation when all pipeline CEs are active, all CEs are not always active from a single-input (image) perspective. This idleness of certain CEs at certain stages (Figure 4b) increases the overall latency, this effect scales with the number of CEs [5], [30]. In practice, there is a trade-off between underutilization and latency. CNNs have tens to hundreds of layers; hence, solving PE underutilization completely may require large numbers of dedicated CEs, resulting in higher latency.

2) *On-chip buffer requirements:* There is a trade-off between on-chip buffer sizes and off-chip memory accesses. This section describes the buffer sizes needed to guarantee minimum off-chip accesses. For generality, we assume weights are stored off-chip at the beginning of a CNN inference. This

is because CNNs may have several millions of weights that cannot always be stored fully on-chip. Consequently, *minimum off-chip accesses* in this context refer to one access per weight and zero access per FM element (apart from the mandatory loads and stores of CNN first and last layers FMs). In *single-CE* case, layers are processed one at a time. Hence, the OFMs are produced completely at the end of each layer. But only a portion of layer weights must be on-chip at a time (See Figure 4a). Equation 4 depicts the estimation of buffer size requirements, where Sz stands for size. The same buffers are reused across layers because layers are processed one at a time. Consequently, the buffering required to achieve the target minimum accesses must accommodate the largest layer FMs, both IFMs and OFMs, plus the largest weights tile. Note that FMs_i must account for multiple copies of the FMs in case a layer has residual connections [15] (e.g., L_2 in Figure 2).

$$\text{BufferSz} = \max_{i=1}^{\text{layers}} (\text{FMsSz}_i) + \max_{i=1}^{\text{layers}} (\text{weightsTileSz}_i) \quad (4)$$

In *pipelined-CEs* case, achieving the defined minimum off-chip accesses requires that all the weights of the pipelined layers be kept on-chip after their first load. Otherwise, as can be inferred from Figure 4b, each weight needs to be accessed as many times as the pipeline stages in which its CE is active. Regarding the FMs, double buffering is required between the CEs to work concurrently. Equation 5 describes the on-chip buffer requirements of pipelined-CEs to guarantee minimum off-chip accesses. Multiplication by 2 is because of double buffering. FMsBufferSz is determined per layer using Multiple-CE builder heuristics. Smaller buffers mean smaller on-chip memory, but less reuse and more weight movement [30], [49].

$$\text{BufferSz} = \sum_{i=1}^{\text{layers}} \left(\text{weightsSz}_i + 2 \times \text{FMsBufferSz}_i \right) \quad (5)$$

This section discussed buffer sizes that guarantee the defined minimum off-chip accesses, assuming unlimited on-chip memory. The following section covers the case where these buffers exceed the available on-chip memory.

3) *Off-chip access:* Equation 6 depicts an example of calculating off-chip accesses of a *single-CE* assuming an OS dataflow (Section II), where $\text{offCh}(x)$ evaluates to 1 if x is

stored off-chip and 0 otherwise. As discussed, we assume that the weights are stored off-chip at the beginning of an inference for generality. Hence, the ideal scenario is when both IFMs and OFMs of a layer fit on-chip, resulting in accesses equal to the size of the weights. The equation also describes two options when the available on-chip memory does not guarantee the ideal scenario. The first option is an output stationary local input stationary. In this option, an IFM element is loaded once from off-chip memory and used to produce all the dependent OFM elements. In this option, the weights need to be loaded multiple times. The second option is output stationary local weight stationary. This option is the opposite of the first, meaning that a weight is loaded once, but an IFM element is loaded multiple times. The adopted option is the one that has fewer memory accesses. Multiple-CE Builder heuristics identify the buffer sizes that minimize accesses in each option.

$$\begin{aligned}
Accesses &= \sum_{i=1}^{layers} Acc(L_i, CE_j) \\
Acc(L_i, CE_j) &= \underset{\text{argmin}}{\left(OFMsSz_i \times \text{offCh}(OFMs_i) + \right.} \\
&\quad \min \left(\text{weightsSz}_i \times \frac{IFMsSz_i}{IFMsBufferSz_j} + \right. \\
&\quad \left. IFMsSz_i, IFMsSz_i \times \frac{\text{weightsSz}_i}{\text{weightsBufferSz}_j} + \right. \\
&\quad \left. \text{weightsSz}_i \right) \times \text{offCh}(IFMs_i) + \\
&\quad \left(1 - \text{offCh}(IFMs_i) \right) \times \text{weightsSz}_i \Big) \\
\text{s.t. } &\text{weightsBufferSz}_j + IFMsBufferSz_j + \max_{i=1}^{layers} (OFMsSz_i \times \\
&\quad (1 - \text{offCh}(OFMs_i))) \leq CE_BufferSz_j
\end{aligned} \tag{6}$$

Equation 7 gives off-chip accesses in the *pipelined-CEs* case where $\text{offCh}(\text{weights}_i, j)$ evaluates to 1 if the weights of the layer are off-chip at the beginning of stage j . As the weights are initially off-chip, $\text{offCh}(\text{weights}_i, 1)$ is always 1. In other stages, the weights of a layer are stored on-chip if the space allows. Each weight that is not kept on-chip after the first load must be accessed as many times as the pipeline stages in which its layer is active (see Figure 4b). In the pipelined-CEs case, the FMs are kept on-chip. This is practically the case when doing tile-grained pipelining, as the buffer sizes are tailored to the available on-chip memory.

$$Accesses = \sum_{i=1}^{CEs} \sum_{j=1}^{CE_Stages_i} \text{weightsSz}_i \times \text{offCh}(\text{weights}_i, j) \tag{7}$$

B. Bottom-up modeling: From blocks to full accelerator

Modeling a multiple-CE accelerator using the models of its building blocks and the interfacing between them is achieved using generalized versions of the equations from the previous

section (Section IV-A) or composite equations formed by substituting some into others. The nature of the modifications to the modeling in the previous section depends on (1) whether the building block processes *one or multiple segments* of a CNN, and (2) whether there is an *inter-segment pipelining* across segments (coarse-grained). This dependency is described in the rest of this section at a high level and clarified using *Segmented* architecture as a concrete example.

1) *Latency and throughput*: Latency and throughput are estimated using the same equations whether the building block processes one or multiple segments. However, the final values differ because when a block processes multiple segments, its PEs, parallelism, and hence utilization are optimized for the average case rather than for a unique segment. The latency and throughput of segments with inter-segment pipelining are estimated similarly to a pipelined-CEs block. However, there is a difference in how the latencies of the pipeline stages are estimated. This is because, in inter-segment pipelining, each stage could comprise a set of CEs rather than one CE and because the granularity is a whole input rather than a tile. The difference between fine and coarse-grained pipelining can be inferred by comparing the Segmented with the Hybrid and SegmentedRR architectures in Figure 2. To account for these differences, equations 2 and 3 are modified in two ways depending on the types of the coarsely-pipelined blocks. For example, in the Segmented case where the coarse-grained blocks are of single-CE type (Figure 2): (1) the stage latency estimation part in Equation 2 is substituted by Equation 1 because each stage is a single-CE processing a set of layers, (2) in Segmented coarse-grained pipeline, each segment processes a distinct image concurrently. Hence, the condition that keeps track of active CEs in Equation 2 must have an additional parameter to identify which CEs are processing the input for which throughput and latency are being estimated. When there is no inter-segment pipelining, the total latency is simply the sum of the segment latencies, and the throughput is the inverse of the latency. In both cases, there is an extra inter-segment communication latency.

2) *On-chip buffer requirements*: When a building block processes multiple segments, the on-chip buffer sizes are estimated considering the worst case, meaning that the buffers must accommodate the largest weight and FM tiles of the layers across these multiple segments. When there is inter-segment pipelining, the interfacing between the segments must apply double-buffering at input granularity between each two segments. Equation 8, which estimates Segmented architecture buffer sizes, clarifies these points. In a Segmented architecture, in principle, a CE could process multiple segments. Hence, $CE_BufferSz_i$ estimation in Equation 8 is simply a generalization of Equation 4, applied across CE segments to account for the worst case. Because Segmented has inter-segment pipelining, there is double-buffering between each two segments ($2 \times \text{interSegBufferSz}_i$).

$$\begin{aligned}
BufferSz &= \sum_{i=1}^{Segments} (CE_BufferSz_i + 2 \times interSegBufferSz_i) \\
CE_BufferSz_i &= \max_{j=1}^{CE_Segments_i} \left(\max_{k=1}^{layers_j} (FMsSz_k) \right) + \\
&\quad \max_{j=1}^{CE_Segments_i} \left(\max_{k=1}^{layers_j} (weightsTileSz_k) \right)
\end{aligned} \tag{8}$$

When there is no inter-segment pipelining, only a single buffer is reused across segments, but to guarantee the defined minimum off-chip accesses, that buffer must accommodate the largest inter-segment intermediate results.

3) *Off-chip access*: Off-chip accesses of a set of segments are the sum of their accesses plus the possible off-chip accesses on the interfacing between them. While the segments' off-chip accesses are computed using the same equations whether the same block processes multiple segments or not, there is an indirect dependency. The accesses depend on the on-chip buffer sizes (see Equations 6, 7), which in turn depend on whether multiple segments are processed using the same block as discussed in Section IV-B2. The off-chip accesses on the interface between the segments depend on the *inter-segment pipelining*. Inter-segment pipelining double-buffering requires more space; when not available on-chip, the data communicated between the segments must be stored and loaded from off-chip. For example, Equation 9 calculates the Segmented architecture off-chip accesses, where $Acc(L_j, CE_i)$ is calculated using Equation 6. Segmented architecture has inter-segment pipelining, and the inter-segment FMs are stored off-chip if the on-chip cannot accommodate them.

$$\begin{aligned}
Accesses &= \sum_{i=1}^{Segments} \left(\left(\sum_{j=1}^{Layers_i} Acc(L_j, CE_i) \right) + 2 \times \right. \\
&\quad \left. interSegBufferSz_i \times offCh(interSegBuffer_i) \right)
\end{aligned} \tag{9}$$

This section used the Segmented architecture as a concrete example. SegmentedRR, Hybrid, or any multiple-CE architecture modeling builds on top of the models of the single-CE and pipelined-CEs similarly, taking into account the impact of single-block processing multiple segments and the existence or absence of inter-segment pipelining.

V. EVALUATION

A. Experimental Setup

1) *Platforms and systems*: Table II shows the FPGA boards used in our evaluation focusing on PEs (DSPs), on-chip memory (Block RAM), and off-chip bandwidth. The boards represent various resource budgets with PEs ranging from hundreds to thousands and on-chip memory ranging from 2.4 to 16 MiB¹. To evaluate the accuracy of MCCM, we use Vitis-IDE (2021.2) to implement and evaluate a set of multiple-CE

¹The on-chip memory values are reported in MiB rather than Mb, which is commonly used by AMD

TABLE II
EVALUATION FPGA BOARDS

	ZC706	VCU108	VCU110	ZCU102
DSPs	900	768	1800	2520
Block RAM(MiB)	2.4	7.6	4	16.6
Off-chip memory BW (GB/s)	3.2	19.2	19.2	19.2

TABLE III
EVALUATED CNN MODELS

	ResNet152	ResNet50	Xception	DenseNet121	MobileNetV2
Abbreviation	Res152	Res50	XCp	Dns121	MobV2
Weights (M)	60.4	25.6	22.9	8.1	3.5
Conv layers	155	53	74	120	52

accelerators using high-level synthesis (HLS). Vitis synthesis results are commonly used both in the literature and as a part of the design process in the industry. MCCM and the evaluation methodology are implemented in Python and C++. The experiments are conducted on a machine with 16 logical cores, Intel(R) Core(TM) i7-10700 CPU @ 2.90GHz.

2) *Workloads*: We use a representative set of CNNs with different structures, depths, and parameter (weight) counts. These are ResNet152 and ResNet50 [15], Xception [10], MobileNetV2 [31], and DenseNet [16]. Table III shows the relevant characteristics of these CNNs. The evaluated CNNs share core blocks with many recent CNNs. For example, MBConv, the core block of MobileNetV2, is used in EfficientNet [35] and MnasNet [34]. The same applies to the Residual blocks of ResNets, and the Extreme Inceptions of Xception are also used in recent CNNs.

3) *Baseline architectures*: To validate MCCM and present a set of use cases, we implement representative accelerators of the three multiple-CE architectures (Section II-C). The Segmented implementation is based on Shen *et al.* [33]. The SegmentedRR tiling and buffer designs and granularity are based on Wei *et al.* [41], and the engine design is based on Ma *et al.* [23]. The implementation of Hybrid architectures is based on Qararyah *et al.* [30]. The experiments use 10 different CE counts in each architecture, starting from 2 CEs (the smallest possible CE count in a multiple-CE accelerator) to 11 CEs. These CE counts cover all possibilities in the baseline architectures. However, MCCM does not impose a limitation on the number of CEs. The number of PEs in a CE depends on the PE budget and is proportional to the CE workload. For example, in a multiple-CE accelerator with 2 CEs on VCU108, the 768 DSPs are distributed on the 2 CEs, and in an accelerator with 11 CEs, the same 768 DSPs are distributed on the 11 CEs.

B. MCCM validation

Table IV summarizes 150 experiments validating MCCM estimation accuracy. The accuracy of the estimation is calculated using Equation 10. MCCM off-chip accesses calculations are exact since the accesses are deterministic and independent of the optimizations of the synthesis. MCCM accuracy ranges from 80.7% to 100%. The average accuracy values are > 90% for the three architectures. Moreover, the average accuracies of the three architectures

TABLE IV
MCCM EVALUATION ACCURACY ON VCU108: SUMMARY OF 150 EXPERIMENTS (3 ARCHITECTURES \times 10 CE COUNTS \times 5 CNNs)

	Max			Min			Average		
	Segmented	SegmentedRR	Hybrid	Segmented	SegmentedRR	Hybrid	Segmented	SegmentedRR	Hybrid
On-chip buffers	99.4%	99.7%	99.8%	84.2%	91.2%	84.6%	93.1%	97.4%	95.4%
Latency	98.8%	99.0%	99.6%	87.2%	80.7%	85.0%	92.8%	93.3%	92.5%
Throughput	99.6%	100%	99.6%	86.4%	83.4%	85.0%	93.9%	95.1%	92.5%
Off-chip accesses	100%	100%	100%	100%	100%	100%	100%	100%	100%

are close to each other; the differences among them are $< 5\%$. There are differences between latency and throughput accuracies in most cases because in multiple-CE accelerators, throughput is not necessarily the inverse of end-to-end latency (Section IV-A1). MCCM correctly predicted the best architecture among the three in 139 of the 150 experiments when considering on-chip buffer sizes, and in all experiments when considering latency, throughput, and accesses. Performance differences between architectures vary greatly and are sensitive to CE count. For example, considering ResNet50, SegmentedRR has the lowest latency of 73% normalized to the latency of Hybrid and 58% normalized to the latency of Segmented when using 2 CEs. In contrast, Hybrid has the lowest latency of 20% normalized to the latency of Segmented and 96% normalized to the latency of SegmentedRR when using 11 CEs.

$$Accuracy = 100 \times \left(1 - \frac{|synthesis\ result - estimated|}{synthesis\ result}\right)\% \quad (10)$$

C. Use Case 1: End-to-end evaluation

TABLE V
MULTIPLE-CE ACCELERATORS THAT ACHIEVE BEST RESULTS (SEGMENTED SEGMENTEDRR HYBRID) AND THEIR CE-COUNTS. MULTIPLE COLORED CELLS IN THE SAME COLUMN FOR THE SAME METRIC INDICATE A TIE. WE CONSIDER RESULTS WITHIN A 10% DIFFERENCE AS A TIE TO ACCOUNT FOR ESTIMATION ERRORS.

	zc706					vcu108					vcu110					zcu102				
	Res152	Res50	XcP	Dns121	MobV2	Res152	Res50	XcP	Dns121	MobV2	Res152	Res50	XcP	Dns121	MobV2	Res152	Res50	XcP	Dns121	MobV2
Latency	2	2	2	3	3	2	2	2	3	3	2	3	3	3	3	2	2	2	4	7
Throughput	3	2	2	4	2	3	2	2	4	3	3	6	4	7	9	4	2	5	11	7
Access	10	11	2	6	10	3	11	2	11	11	2	2	2	2	2	8	3	7	3	7
Buffers	2	2	2	2	2	2	2	2	2	2	2	2	2	2	2	2	2	2	2	2

This use case discusses MCCM end-to-end evaluation of the baseline multiple-CE architectures. Table V depicts a summary of this evaluation. It shows MCCM selection of the accelerators that achieve the best results considering different metrics, CNNs, and FPGA boards. Four insights can be identified by examining Table V. *First*, in 80% of the cases, no single architecture provides the best results in the four metrics, even for the same CNN model and board. This is shown in the table

as 16 out of 20 columns do not have four cells of the same color. The 4 cases where Hybrid is best in all metrics belong to MobV2 and XcP, these CNNs have various convolution types. This is expected as Hybrid architecture was proposed to handle such CNNs [30]. *Second*, even when a single architecture yields the best results in all metrics, no single instance of that architecture is always the best. For example, for MobV2 on ZC706 (fifth column), the Hybrid accelerator of 2 CEs has the best latency and throughput, the one with 6 CEs has the minimum off-chip accesses, and the one with 11 CEs has the minimum buffer requirements. *Third*, some metrics are uniquely dominated by one of the architectures. For example, SegmentedRR achieves the best latency in 15 out of 20 cases. This is because SegmentedRR architectures were proposed to minimize latency [38], [41]. Hybrid has the lowest buffer requirements in 14 out of 20 cases. *Fourth*, the Hybrid always achieves the minimum off-chip accesses as this was one of its design objectives [30]. The other two architectures catch up on VCU108 and VCU110, as these boards have relatively large on-chip memories that accommodate big enough buffers required to achieve the minimum off-chip access (Table II). *In summary*, multiple-CE accelerators' different CE arrangements affect their performance and efficiency, as discussed in detail in sections IV-A and IV-B. This highlights the importance of exploring different CE arrangement possibilities and identifying the best ones considering the CNN models, hardware resources, and the metric of interest.

D. Use Case 2: Fine-grained evaluation

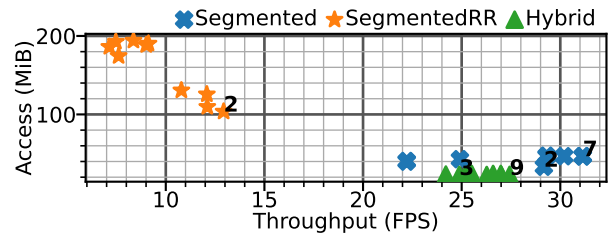


Fig. 5. Throughput vs. off-chip memory accesses of ResNet50 on ZC706 using 10 accelerator instances per architecture with 2-11 CEs. The numbers indicate the CE counts of the accelerators with the highest throughput or minimum accesses of each architecture.

This use case demonstrates MCCM *fine-grained* evaluation to identify the performance bottlenecks of multiple-CE architectures and guide optimizations that alleviate these bottlenecks. Figure 5 depicts MCCM estimations of throughput and off-chip accesses of the three baseline architectures. As can

be seen, both Hybrid and Segmented have relatively good results in both metrics. SegmentedRR instances, however, have considerably more off-chip memory accesses that form a bottleneck. Figure 6a shows MCCM breakdown of compute and memory access time of SegmentedRR with 2 CEs, which has the highest throughput among SegmentedRR in Figure 5. In segments 22–26, the memory access time is the bottleneck. In 29% of the overall execution time, CEs are idle, waiting for data. The Segmented and Hybrid, by contrast, have no such bottlenecks. For example, the breakdown of compute and memory access time of Segmented with 7 CEs, which has the highest throughput among Segmented, is shown in Figure 6b.

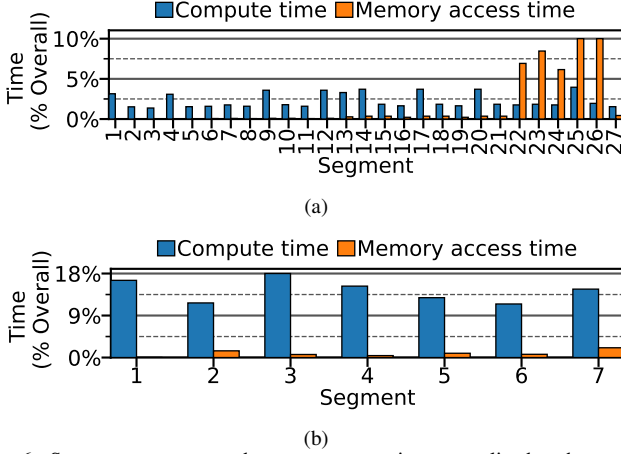


Fig. 6. Segments compute and memory access time normalized to the overall execution time of (a) SegmentedRR with 2 CEs, (b) Segmented with 7 CEs using ResNet50 on ZC706

When considering alleviating the off-chip access bottleneck, data compression is a candidate optimization [8]. However, compression has its overhead. MCCM fine-grained evaluation helps identify the segments that form bottlenecks and apply compression only to these segments' layers to ensure minimum overheads. For example, Figure 6a suggests that compression would be beneficial only for the layers of segments 22 – 26. Moreover, it is crucial to identify which data dominates the accesses. For example, Figure 7 shows MCCM breakdown of the accesses of the accelerator instances with the highest throughput in each of the three architectures shown in Figure 5. Figure 7 suggests that while in SegmentedRR and Hybrid cases, compressing the weights would have a considerable impact on the accesses, compressing FM would be a pure overhead.

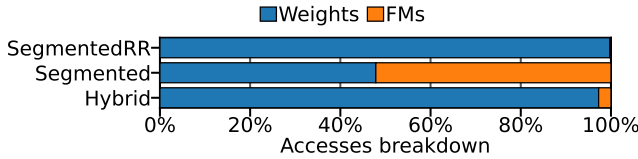


Fig. 7. Off-chip memory accesses breakdown of SegmentedRR with 2 CEs, Segmented with 7 CEs, and Hybrid with 9 CEs using ResNet50 on ZC706.

E. Use Case 3: Guiding design space exploration

This use case demonstrates how MCCM fast evaluation enables a systematic multiple-CE accelerator design approach based on identifying the performance bottlenecks and exploring the space of design points that alleviate these bottlenecks. This use case aims to identify the architecture of a multiple-CE accelerator that maximizes throughput while minimizing on-chip memory usage. The CNN and board used are XCp and VCU110. Figure 8 shows the trade-off between throughput and on-chip buffer requirements using XCp on VCU110.

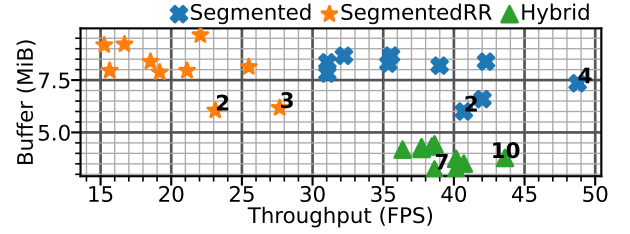


Fig. 8. Throughput vs. on-chip buffer using XCp on VCU110 using 10 accelerator instances per architecture with 2-11 CEs. The numbers indicate the CE counts of the accelerators with the highest throughput or minimum buffer requirements of each architecture.

One way to derive multiple-CE architectures with better throughput-buffer trade-offs is to take the most promising architectures in each metric as starting points, identify their bottlenecks using MCCM fine-grained evaluation, and explore architectures that mitigate these bottlenecks. The most promising architectures in Figure 8 are those located in the bottom right region. For example, the Segmented accelerator with 4 CEs has the highest throughput, and the Hybrid with 7 CEs has the lowest buffer requirements.

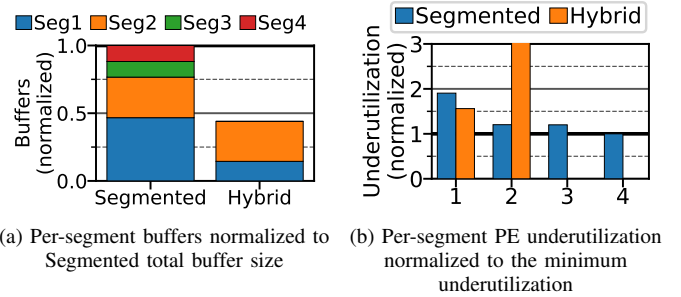


Fig. 9. Buffer and PE underutilization of Hybrid with 7 CEs (2 segments) and Segmented with 4 CEs (4 segments)

Figure 9 depicts MCCM evaluation of the bottlenecks of the two mentioned instances of Segmented and Hybrid architectures. As Figure 9a shows, the buffers of the first segments of the Segmented form a bottleneck. The opposite is the case for Hybrid. Regarding throughput, both Hybrid and Segmented have coarse-grained pipelining (Section IV-B). Hence, their throughput is determined by the slowest segment execution time. MCCM breakdown shows that the first block is the bottleneck in the case of Segmented, but the last block is the bottleneck in the case of Hybrid. The main reason behind

that is the PE underutilization shown in Figures 9b. The higher the PE underutilization is, the slower the block.

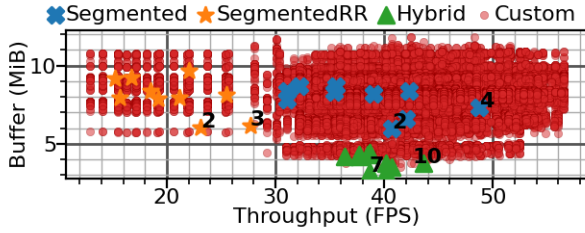


Fig. 10. Throughput vs. on-chip buffer using XCp on VCU110 of a sample of 100000 custom accelerators

The observation that the bottlenecks are in the Segmented first block and Hybrid second block hints that a custom architecture that comprises a Hybrid-like first block followed by Segmented-like blocks may improve efficiency. Assuming 10 CE possibilities (2-11 CEs) and given the XCp model structure, the design space of such custom architecture has roughly *97.1 billion* designs. Figure 10 shows an evaluation of a random sample of 100000 out of them. MCCM evaluation of this sample took 10.5 minutes with an average of *6.3 ms* per design. The average synthesis time of a single design on the same machine is roughly an hour, meaning that MCCM is in the order of *100000*× faster. Traditional synthesis-based evaluation of the sample of 100000 designs would take *years*. Exploring the selected sample resulted in identifying custom accelerators that outperform the state-of-the-art. Some custom accelerators achieve the throughput of the Segmented with 4 CEs while reducing the buffer requirements by up to 48%. Custom accelerators with the highest throughput improve throughput by up to 17% compared to Segmented with 4 CEs while reducing buffer requirements by up to 39%.

VI. RELATED WORK

The literature on DL accelerator design suggests that no fixed architecture is optimal given the diverse workloads and application requirements and that model-aware CNN, and DNN in general, to hardware mappings achieve the best performance and efficiency [3]–[5], [18], [26]. The prior art on optimizing CNN to hardware mapping takes two main forms. The first form focuses on intra-layer optimizations, including dataflow and reuse, parallelism strategies, tiling, and exploring custom algorithms like GEMM and FFT [7], [9], [17]–[19], [22], [23], [26]. Timeloop [26] and MAESTRO [18] provide frameworks for evaluating and exploring the intra-layer architecture design space. The second form focuses on inter-layer or model-level optimizations, including designing layer-dedicated compute engines (CEs), convolution layer-fusion, and inter-layer pipelining [3], [6], [14], [28], [37], [44], [49].

FPGAs are a common target for inter-layer optimizations due to their reconfigurability, which enables arranging the resources into a custom number of dedicated CEs. When designing a multiple-CE accelerator, there are numerous CE

arrangement possibilities. An obvious arrangement is a set of layer-specific and fully pipelined CEs where the number of CEs is equal to the number of CNN layers [3], [37], [49]. More scalable, resource and latency-aware arrangements have an adjustable number of CEs, which is determined by both the CNN structure and the hardware budget [1], [5], [25], [30], [32], [33], [38], [41], [50].

The prior art multiple-CE accelerators follow a set of fixed design templates and are not based on systematic design space exploration. This paper proposes a multiple-CE accelerator analytical cost model and a fast evaluation methodology based on this model. Fast evaluation of multiple-CE architectures is key to a systematic design approach.

VII. CONCLUSION

Multiple-CE accelerators are more adaptable to various CNN model structures and application performance metrics than generic accelerators. However, existing multiple-CE accelerators have fixed architectures and do not explore the impact of CE arrangements on performance and efficiency. This paper proposed Multiple-CE accelerator analytical Cost Model (MCCM), and a fast MCCM-based evaluation methodology. MCCM is in the order of *100000*× faster than traditional synthesis-based evaluation and has an average accuracy of *> 90%*. MCCM helps to identify the best-performing among state-of-the-art multiple-CE accelerators given various metrics, CNNs, and resource budgets. Moreover, MCCM fast evaluation permits identifying performance bottlenecks and exploring the vast space of CE arrangements, opening the door to a more systematic approach to multiple-CE accelerator design.

REFERENCES

- [1] M. Alwani, H. Chen, M. Ferdman, and P. Milder, “Fused-layer cnn accelerators,” in *2016 49th Annual IEEE/ACM International Symposium on Microarchitecture (MICRO)*. IEEE, 2016, pp. 1–12.
- [2] L. Bai, Y. Zhao, and X. Huang, “A cnn accelerator on fpga using depthwise separable convolution,” *IEEE Transactions on Circuits and Systems II: Express Briefs*, vol. 65, no. 10, pp. 1415–1419, 2018.
- [3] M. Blott, T. B. Preußner, N. J. Fraser, G. Gambardella, K. O’Brien, Y. Umuroglu, M. Leeser, and K. Vissers, “Finn-r: An end-to-end deep-learning framework for fast exploration of quantized neural networks,” *ACM Transactions on Reconfigurable Technology and Systems (TRETS)*, vol. 11, no. 3, pp. 1–23, 2018.
- [4] A. Boroumand, S. Ghose, B. Akin, R. Narayanaswami, G. F. Oliveira, X. Ma, E. Shiu, and O. Mutlu, “Google neural network models for edge devices: Analyzing and mitigating machine learning inference bottlenecks,” in *2021 30th International Conference on Parallel Architectures and Compilation Techniques (PACT)*. IEEE, 2021, pp. 159–172.
- [5] X. Cai, Y. Wang, X. Ma, Y. Han, and L. Zhang, “Deepburning-seg: Generating dnn accelerators of segment-grained pipeline architecture,” in *2022 55th IEEE/ACM International Symposium on Microarchitecture (MICRO)*. IEEE, 2022, pp. 1396–1413.
- [6] X. Cai, Y. Wang, and L. Zhang, “Optimus: towards optimal layer-fusion on deep learning processors,” in *Proceedings of the 22nd ACM SIGPLAN/SIGBED International Conference on Languages, Compilers, and Tools for Embedded Systems*, 2021, pp. 67–79.
- [7] Y.-H. Chen, J. Emer, and V. Sze, “Eyeriss: A spatial architecture for energy-efficient dataflow for convolutional neural networks,” *ACM SIGARCH computer architecture news*, vol. 44, no. 3, pp. 367–379, 2016.
- [8] Y.-H. Chen, T.-J. Yang, J. Emer, and V. Sze, “Eyeriss v2: A flexible accelerator for emerging deep neural networks on mobile devices,” *IEEE Journal on Emerging and Selected Topics in Circuits and Systems*, vol. 9, no. 2, pp. 292–308, 2019.

- [9] S. Chetlur, C. Woolley, P. Vandermersch, J. Cohen, J. Tran, B. Catanzaro, and E. Shelhamer, "cudnn: Efficient primitives for deep learning," *arXiv preprint arXiv:1410.0759*, 2014.
- [10] F. Chollet, "Xception: Deep learning with depthwise separable convolutions," in *Proceedings of the IEEE conference on computer vision and pattern recognition*, 2017, pp. 1251–1258.
- [11] Z. Choudhury, S. Shrivastava, L. Ramapantulu, and S. Purini, "An fpga overlay for cnn inference with fine-grained flexible parallelism," *ACM Transactions on Architecture and Code Optimization (TACO)*, vol. 19, no. 3, pp. 1–26, 2022.
- [12] E. Chung, J. Fowers, K. Ovtcharov, M. Papamichael, A. Caulfield, T. Massengill, M. Liu, D. Lo, S. Alkalay, M. Haselman *et al.*, "Serving dnn in real time at datacenter scale with project brainwave," *IEEE Micro*, vol. 38, no. 2, pp. 8–20, 2018.
- [13] J. Fowers, K. Ovtcharov, M. Papamichael, T. Massengill, M. Liu, D. Lo, S. Alkalay, M. Haselman, L. Adams, M. Ghandi *et al.*, "A configurable cloud-scale dnn processor for real-time ai," in *2018 ACM/IEEE 45th Annual International Symposium on Computer Architecture (ISCA)*. IEEE, 2018, pp. 1–14.
- [14] M. Gao, X. Yang, J. Pu, M. Horowitz, and C. Kozyrakis, "Tangram: Optimized coarse-grained dataflow for scalable nn accelerators," in *Proceedings of the Twenty-Fourth International Conference on Architectural Support for Programming Languages and Operating Systems*, 2019, pp. 807–820.
- [15] K. He, X. Zhang, S. Ren, and J. Sun, "Deep residual learning for image recognition," in *Proceedings of the IEEE conference on computer vision and pattern recognition*, 2016, pp. 770–778.
- [16] G. Huang, Z. Liu, L. Van Der Maaten, and K. Q. Weinberger, "Densely connected convolutional networks," in *Proceedings of the IEEE conference on computer vision and pattern recognition*, 2017, pp. 4700–4708.
- [17] S.-C. Kao and T. Krishna, "Gamma: Automating the hw mapping of dnn models on accelerators via genetic algorithm," in *Proceedings of the 39th International Conference on Computer-Aided Design*, 2020, pp. 1–9.
- [18] H. Kwon, P. Chatarasi, M. Pellauer, A. Parashar, V. Sarkar, and T. Krishna, "Understanding reuse, performance, and hardware cost of dnn dataflow: A data-centric approach," in *Proceedings of the 52nd Annual IEEE/ACM International Symposium on Microarchitecture*, 2019, pp. 754–768.
- [19] A. Lavin and S. Gray, "Fast algorithms for convolutional neural networks," in *Proceedings of the IEEE conference on computer vision and pattern recognition*, 2016, pp. 4013–4021.
- [20] Y. LeCun, Y. Bengio, and G. Hinton, "Deep learning," *nature*, vol. 521, no. 7553, pp. 436–444, 2015.
- [21] Y. LeCun, K. Kavukcuoglu, and C. Farabet, "Convolutional networks and applications in vision," in *Proceedings of 2010 IEEE international symposium on circuits and systems*. IEEE, 2010, pp. 253–256.
- [22] W. Lu, G. Yan, J. Li, S. Gong, Y. Han, and X. Li, "Flexflow: A flexible dataflow accelerator architecture for convolutional neural networks," in *2017 IEEE International Symposium on High Performance Computer Architecture (HPCA)*. IEEE, 2017, pp. 553–564.
- [23] Y. Ma, Y. Cao, S. Vrudhula, and J.-s. Seo, "Optimizing the convolution operation to accelerate deep neural networks on fpga," *IEEE Transactions on Very Large Scale Integration (VLSI) Systems*, vol. 26, no. 7, pp. 1354–1367, 2018.
- [24] Y. Ma, N. Suda, Y. Cao, J.-s. Seo, and S. Vrudhula, "Scalable and modularized rtl compilation of convolutional neural networks onto fpga," in *2016 26th international conference on field programmable logic and applications (FPL)*. IEEE, 2016, pp. 1–8.
- [25] D. T. Nguyen, H. Kim, and H.-J. Lee, "Layer-specific optimization for mixed data flow with mixed precision in fpga design for cnn-based object detectors," *IEEE Transactions on Circuits and Systems for Video Technology*, vol. 31, no. 6, pp. 2450–2464, 2020.
- [26] A. Parashar, P. Raina, Y. S. Shao, Y.-H. Chen, V. A. Ying, A. Mukkara, R. Venkatesan, B. Khailany, S. W. Keckler, and J. Emer, "Timeloop: A systematic approach to dnn accelerator evaluation," in *2019 IEEE international symposium on performance analysis of systems and software (ISPASS)*. IEEE, 2019, pp. 304–315.
- [27] L. Petrica, T. Alonso, M. Kroes, N. Fraser, S. Cotofana, and M. Blott, "Memory-efficient dataflow inference for deep cnns on fpga," in *2020 International Conference on Field-Programmable Technology (ICFPT)*. IEEE, 2020, pp. 48–55.
- [28] F. Qararyah, M. W. Azhar, M. A. Maleki, and P. Trancoso, "Fusing depthwise and pointwise convolutions for efficient inference on gpus," in *Workshop Proceedings of the 53rd International Conference on Parallel Processing*, 2024, pp. 58–67.
- [29] F. Qararyah, M. W. Azhar, and P. Trancoso, "Fibha: Fixed budget hybrid cnn accelerator," in *2022 IEEE 34th International Symposium on Computer Architecture and High Performance Computing (SBAC-PAD)*. IEEE, 2022, pp. 180–190.
- [30] F. Qararyah, M. W. Azhar, and P. Trancoso, "An efficient hybrid deep learning accelerator for compact and heterogeneous cnns," *ACM Transactions on Architecture and Code Optimization*, vol. 21, no. 2, pp. 1–26, 2024.
- [31] M. Sandler, A. Howard, M. Zhu, A. Zhmoginov, and L.-C. Chen, "Mobilenetv2: Inverted residuals and linear bottlenecks," in *Proceedings of the IEEE conference on computer vision and pattern recognition*, 2018, pp. 4510–4520.
- [32] Y. Shen, M. Ferdman, and P. Milder, "Overcoming resource underutilization in spatial cnn accelerators," in *2016 26th International Conference on field programmable logic and applications (FPL)*. IEEE, 2016, pp. 1–4.
- [33] Y. Shen, M. Ferdman, and P. Milder, "Maximizing cnn accelerator efficiency through resource partitioning," in *2017 ACM/IEEE 44th Annual International Symposium on Computer Architecture (ISCA)*. IEEE, 2017, pp. 535–547.
- [34] M. Tan, B. Chen, R. Pang, V. Vasudevan, M. Sandler, A. Howard, and Q. V. Le, "Mnasnet: Platform-aware neural architecture search for mobile," in *Proceedings of the IEEE/CVF conference on computer vision and pattern recognition*, 2019, pp. 2820–2828.
- [35] M. Tan and Q. Le, "Efficientnet: Rethinking model scaling for convolutional neural networks," in *International conference on machine learning*. PMLR, 2019, pp. 6105–6114.
- [36] Y. Umuroglu, N. J. Fraser, G. Gambardella, M. Blott, P. Leong, M. Jahre, and K. Vissers, "Finn: A framework for fast, scalable binarized neural network inference," in *Proceedings of the 2017 ACM/SIGDA international symposium on field-programmable gate arrays*, 2017, pp. 65–74.
- [37] S. I. Venieris and C.-S. Bouganis, "fpgaconvnet: A framework for mapping convolutional neural networks on fpgas," in *2016 IEEE 24th Annual International Symposium on Field-Programmable Custom Computing Machines (FCCM)*. IEEE, 2016, pp. 40–47.
- [38] S. I. Venieris and C.-S. Bouganis, "Latency-driven design for fpga-based convolutional neural networks," in *2017 27th International Conference on Field Programmable Logic and Applications (FPL)*. IEEE, 2017, pp. 1–8.
- [39] S. I. Venieris and C.-S. Bouganis, "fpgaconvnet: Mapping regular and irregular convolutional neural networks on fpgas," *IEEE transactions on neural networks and learning systems*, vol. 30, no. 2, pp. 326–342, 2018.
- [40] S. I. Venieris, C.-S. Bouganis, and N. D. Lane, "Multiple-deep neural network accelerators for next-generation artificial intelligence systems," *Computer*, vol. 56, no. 3, pp. 70–79, 2023.
- [41] X. Wei, Y. Liang, X. Li, C. H. Yu, P. Zhang, and J. Cong, "Tgpa: Tile-grained pipeline architecture for low latency cnn inference," in *2018 IEEE/ACM International Conference on Computer-Aided Design (ICCAD)*. ACM, 2018, pp. 1–8.
- [42] D. Wu, Y. Zhang, X. Jia, L. Tian, T. Li, L. Sui, D. Xie, and Y. Shan, "A high-performance cnn processor based on fpga for mobilenets," in *2019 29th International Conference on Field Programmable Logic and Applications (FPL)*. IEEE, 2019, pp. 136–143.
- [43] M. Xia, Z. Huang, L. Tian, H. Wang, V. Chang, Y. Zhu, and S. Feng, "Sparknoc: An energy-efficiency fpga-based accelerator using optimized lightweight cnn for edge computing," *Journal of Systems Architecture*, vol. 115, p. 101991, 2021.
- [44] Y. Yang, J. S. Emer, and D. Sanchez, "Isosceles: Accelerating sparse cnns through inter-layer pipelining," in *2023 IEEE International Symposium on High-Performance Computer Architecture (HPCA)*. IEEE, 2023, pp. 598–610.
- [45] H. Ye, X. Zhang, Z. Huang, G. Chen, and D. Chen, "Hybridcnn: A framework for high-performance hybrid dnn accelerator design and implementation," in *2020 57th ACM/IEEE Design Automation Conference (DAC)*. IEEE, 2020, pp. 1–6.
- [46] Z. Yu and C.-S. Bouganis, "Auto ws: Automate weights streaming in layer-wise pipelined dnn accelerators," in *2024 Design, Automation & Test in Europe Conference & Exhibition (DATE)*. IEEE, 2024, pp. 1–6.
- [47] C. Zhang, P. Li, G. Sun, Y. Guan, B. Xiao, and J. Cong, "Optimizing fpga-based accelerator design for deep convolutional neural networks,"

- in *Proceedings of the 2015 ACM/SIGDA international symposium on field-programmable gate arrays*, 2015, pp. 161–170.
- [48] D. Zhang, S. Huda, E. Songhori, K. Prabhu, Q. Le, A. Goldie, and A. Mirhoseini, “A full-stack search technique for domain optimized deep learning accelerators,” in *Proceedings of the 27th ACM International Conference on Architectural Support for Programming Languages and Operating Systems*, 2022, pp. 27–42.
- [49] X. Zhang, J. Wang, C. Zhu, Y. Lin, J. Xiong, W.-m. Hwu, and D. Chen, “Dnnbuilder: An automated tool for building high-performance dnn hardware accelerators for fpgas,” in *2018 IEEE/ACM International Conference on Computer-Aided Design (ICCAD)*. IEEE, 2018, pp. 1–8.
- [50] X. Zhang, H. Ye, J. Wang, Y. Lin, J. Xiong, W.-m. Hwu, and D. Chen, “Dnnexplorer: a framework for modeling and exploring a novel paradigm of fpga-based dnn accelerator,” in *Proceedings of the 39th International Conference on Computer-Aided Design*, 2020, pp. 1–9.